Journal of Quantitative Spectroscopy & Radiative Transfer 305 (2023) 108624

Contents lists available at ScienceDirect

Journal of Quantitative Spectroscopy & Radiative Transfer

journal homepage: www.elsevier.com/locate/jqsrt

Computational, rotational and ro-vibrational experimental investigation of monodeuterated chloromethane

Andrea Pietropolli Charmet[a,*], Paolo Stoppa[a], Alessandra De Lorenzi[a], Mattia Melosso[b,c], Andrè Achilli[b], Luca Dore[b], Cristina Puzzarini[b], Elisabetta Canè[d], Filippo Tamassia[d]

[a] Dipartimento di Scienze Molecolari e Nanosistemi, Università Ca' Foscari Venezia, Via Torino 155, Mestre, VE 30172, Italy
[b] Dipartimento di Chimica "Giacomo Ciamician", Università di Bologna, Via F. Selmi 2, Bologna 40126, Italy
[c] Scuola Superiore Meridionale, Largo San Marcellino 10, Naples 80136, Italy
[d] Dipartimento di Chimica Industriale "Toso Montanari", Università di Bologna, Viale del Risorgimento 4, Bologna 40136, Italy

ARTICLE INFO

Article history:
Received 28 February 2023
Revised 18 April 2023
Accepted 18 April 2023
Available online 19 April 2023

Keywords:
Monodeuterated chloromethane
Infrared spectrum
Ab initio calculations
Vibrational analysis
Rotational spectrum

ABSTRACT

In the present work, a combined theoretical and spectroscopic characterization of the different isotopologues of mono-deuterated chloromethane, CH_2DCl, has been carried out in order to provide reliable spectroscopic data to support and guide future studies. State-of-the-art *ab initio* calculations were performed to derive accurate predictions of equilibrium structure, rotational constants, and centrifugal distortion terms. The rotational spectra of the ^{13}C species have been recorded for the first time in the 250–300 GHz frequency range and, for the two isotopologues $^{12}CH_2D^{35}Cl$ and $^{12}CH_2D^{37}Cl$, the knowledge has been extended up to 520 GHz. The observed transitions have been analyzed with a Watson-type Hamiltonian and allowed the determination of several spectroscopic parameters, all in excellent agreement with our computed values. These new experimental and computed data, combined with the ones previously available in the literature, led to the determination of an accurate and complete semi-experimental (SE) equilibrium structure for chloromethane. The medium resolution (up to 0.1 cm^{-1}) gas-phase infrared spectra of CH_2DCl were investigated in the region 600–9000 cm^{-1}. All the most important spectral features were assigned in terms of fundamental, overtone and combination bands, thus obtaining an accurate description of the vibrational structure. Several polyads involving different vibrational levels were identified and disentangled with the aid of our computed high-level hybrid force field.

1. Introduction

Chlorinated volatile organic compounds (Cl-VOCs) play a significant role in the Earth's atmosphere, since they can act as greenhouse gasses and sources of reactive chlorine in the troposphere thus leading to stratospheric ozone destruction [1], and also as environmentally hazardous trace gasses (see for example Refs. [2–4], and references therein). Their sources are either natural or due to different anthropogenic processes. Highly accurate real-time detection and monitoring of trace gas pollutants are made possible by recent improvements in high-resolution spectroscopies [5–7], but these techniques rely on the availability of the corresponding spectroscopic data [8]. These data are generally obtained by accurate line-shape and ro-vibrational analyses of infrared spectra, often requiring a proper treatment of resonances. The corresponding coupling parameters as well as other relevant spectroscopic parameters (band positions, intensities, rotational constants, and so on) can be nowadays accurately predicted by state-of-the art quantum-mechanical computations [9–12] thus greatly supporting the experimental analysis in disentangling the complex vibrational and rovibrational features of chlorinated trace gas compounds [13–17].

The first detection of chloromethane (methyl chloride, CH_3Cl) in the Earth's atmosphere has been achieved by the analysis of the strong ν_1 band around 3.4 μm [18], and its global distribution (in both the upper troposphere and lower stratosphere) has been then successfully measured by the ACE-FTS experiment [19,20]. Among the several Cl-VOCs, chloromethane, with local atmospheric concentration values that can be well above 1000 pptv over some regions [21] and an averaged concentration estimated in the 553−559 pptv range (see the latest assessment on Stratospheric Ozone [1]), is considered a very relevant one, accounting for almost 17% of the total reactive chlorine in the troposphere. Besides the oceans, its natural sources comprise plants [22], soils [23,24] and wildfires [25]. The anthropogenic processes involved in the emissions of CH_3Cl are mainly chemical activities [26] and biomass burning [25]; it is worthwhile to note that recently CH_3Cl has been detected also in the human breath [27]. These close correlations between its presence in the atmosphere and the

* Corresponding author.
E-mail address: jacpnike@unive.it (A. Pietropolli Charmet).

https://doi.org/10.1016/j.jqsrt.2023.108624

biological/anthropogenic activities make CH_3Cl a promising biomarker to be used for the search of potentially hospitable exoplanets [28]. For all these reasons, chloromethane has been the subject of several high-resolution infrared spectroscopic studies focused on line-positions and line-shape parameters (see, for example, Refs. [29–38], and references therein) as well as theoretical investigations (see for example Refs. [39–42], and references therein), while the analysis of its microwave spectra provided accurate values for the ground state constants [43,44].

In comparison to the diversity and richness of chlorinated compounds present in the Earth's atmosphere, until few years ago it was generally assumed that in the interstellar medium chlorinated molecules could be present only in the form of simple chlorinated hydrides [45]. The recent finding of chloromethane, with the unambiguously assignment of signals coming from both the two chlorine isotopologues, in the protostar IRAS 16,293–2422 and in the coma of comet 67P/Churyumov-Gerasimenko by the Rosetta mission [46] was groundbreaking since it provided evidence of an interplay between halogens and organic interstellar chemistry. This discovery thus highlighted that also the chemistry of organohalides needs to be properly considered in the planet-forming regions, and therefore stimulated recent investigations of other possible candidates [47,48], and of their formation [49]. The fact that in the same protostar many deuterated and bi-deuterated species have been detected (HDO/D_2O [50], NHD/ND_2 [51,52], and CH_2DCN/ CHD_2CN [53]) points out that also CH_2DCl (the monodeuterated form of chloromethane) might be present. Anyway, accurate spectroscopic data are needed for its detection and for the determination of the $CH_2D^{35}Cl/CH_2D^{37}Cl$ ratio [54]. Until recently, only some bands of $CH_2D^{35}Cl$ were investigated by high-resolution spectroscopy [55–57]. Therefore, we decided to assist and drive the search of monodeuterated chloromethane (both the $CH_2D^{35}Cl$ and $CH_2D^{37}Cl$ isotopologues) in the interstellar medium by providing the necessary laboratory data and theoretical predictions. As a first step, we determined precise rest frequencies at mm-wavelengths and accurate ground state constants for both the chlorine isotopologues [58]. Then, for $CH_2D^{37}Cl$ we performed the ro-vibrational analysis of the bands falling in the 15.4–9.3 μm region, i.e. the ν_5, ν_6 and ν_9 fundamentals [59].

In the present work, we carried out a complete experimental analysis of the vibrational spectrum of mono-deuterated chloromethane in the region 600–9000 cm^{-1} in combination with an accurate quantum-chemical characterization. The employed approach provided accurate predictions of the spectroscopic parameters for vibrational ground and excited states and assisted the assignments of the absorption features in terms of fundamentals, overtone and combination bands up to three quanta. In addition, from the analysis of the millimeter-wave spectra, we derived an accurate set of spectroscopic parameters for both $^{13}CH_2D^{35}Cl$ and $^{13}CH_2D^{37}Cl$ species. We also extended the measurements of the rotational spectrum of the two main species at submillimeter-wavelengths (up to 520 GHz) with the aim of expanding the analysis to higher-order centrifugal terms. Finally, using these new data in combination with computed vibration-rotation interaction constants we were able to determine a complete semi-experimental (SE) equilibrium molecular structure for chloromethane, whose parameters are in excellent agreement with those obtained from *ab initio* calculations. The results reported here, combined with the previous ones, constitute a solid base of reliable spectroscopic data on mono-deuterated chloromethane species to assist and guide their search in remote environments as well as to support future high-resolution studies in the infrared region. The spectroscopic parameters and the Coriolis terms here reported will greatly help the ro-vibrational analysis of the most relevant absorptions and the treatment of the interactions between different excited vibrational levels.

2. Experimental details

The CH_2DCl sample, with natural isotopic composition, was prepared by reacting monodeuterated methanol (CDN Isotopes, 99.2% D-enriched) with NaCl in a solution of diluted sulphuric acid, following the method previously described [55].

The gas-phase room temperature infrared spectra at medium resolution (from 1.0 up to 0.2 cm^{-1}) were measured at Ca' Foscari University of Venice (Italy), using a Bruker Vertex 70 FTIR instrument [14,15], and using a combination of different cells, sources and beam-splitters according to the spectral region investigated. In the region 600–6500 cm^{-1}, a KBr beam-splitter in conjunction with a cell having a path length of 0.16 m and a Globar source were employed, while the sample pressures were in the 1.5–60 kPa range. In addition, in the region between 5000 and 9000 cm^{-1}, some spectra were recorded also using a quartz beam-splitter together with a tungsten lamp and a multi-pass cell (with a total optical path length of 37.5 m). During these measurements the sample pressure was kept at 2.1 kPa.

Additional gas-phase infrared spectra were recorded at 0.1 and 0.5 cm^{-1} resolution at the Department of Industrial Chemistry "Toso Montanari" of University of Bologna (Italy), using a Bomem DA3.002 FTIR spectrometer [60,61] equipped with a Globar source, a KBr beam-splitter, a mercury cadmium telluride (MCT) and an InSb detectors. The spectra were recorded at different pressures, ranging from 13.3 to 13,330 Pa, and two different pathlengths, 0.16 and 8 m. The total spectral range spanned was 450–5500 cm^{-1}. Several hundred scans were co-added in order to improve the signal-to-noise ratio.

The rotational spectra of $CH_2D^{35}Cl$ and $CH_2D^{37}Cl$, as well as their ^{13}C-counterparts, have been recorded with the frequency-modulation millimeter-/submillimeter-wave spectrometer at the Department of Chemistry "Giacomo Ciamician" of the University of Bologna (Italy) [62,63]. For the present measurements, a Gunn diode operating in the 80–115 GHz range coupled to passive frequency multipliers (tripler, quadrupler, and sextupler) has been used as radiation source. The frequency of the Gunn's radiation is stabilized in a phase-lock loop and sine-wave modulated at a frequency of $f = 48$ kHz. All the electronics employed in the phase-lock loop are referenced to a rubidium atomic clock that ensures the frequency accuracy of the spectra recorded. The radiation is fed into a 3 m long glass absorption cell containing vapors of pure CH_2DCl at a pressure between 0.27 and 2.7 Pa (depending on the intensity of the transitions to be observed). The output signal is finally detected by a zero-bias Schottky diode before being amplified, filtered, and demodulated at twice the modulation frequency by a lock-in amplifier.

3. Computational details

Accurate prediction of the equilibrium structure parameters was obtained by exploiting the CCSD(T)/CBS+CV+fT+fQ composite scheme. The definition of this model starts from CCSD(T)/CBS+CV (hereafter CBS+CV), which is obtained by exploiting the so-called "gradient" scheme approach [64,65]. CCSD(T) [66] stands for coupled-cluster (CC) singles and doubles augmented by a perturbative treatment of triple excitation. The CFOUR suite of programs [67,68] was used for these computations. In the extrapolation procedure, we employed different correlation consistent Dunning basis sets [69–71]: for the H and C atoms we used the cc-pVnZ (n = T, Q, 5) basis sets, while for Cl atom their augmented counterparts were employed with an extra hard d function (i.e., aug-cc-pV(n+d)Z) to take into account inner-shell polarization effects; to compute the core-valence (CV) correlation term, we used the cc-pCVQZ basis set [72]. The CBS+CV structure has been obtained by minimizing the

Table 1
Comparison between theoretical (THEO) and semi-experimental (SE) equilibrium structural parameters of CH_3Cl.

	THEO				SE	
	CBS+CV[a]	CBS_{best}[a]	Ref. 43[b]	Ref. 89[c]	This work[d]	Ref. 97[d]
r (C–H)	1.0832	1.0833	1.0834	1.0838	1.083450(8)	1.0842(2)
r (C–Cl)	1.7768	1.7777	1.7777	1.7772	1.777725(5)	1.7768(2)
β (H–C-Cl)	108.40	108.39	108.38	108.45	108.3740(9)	108.72
β (H–C-H)	110.53	110.53	110.54	110.48	110.5458(9)	110.21(3)

[a] This work. CBS+CV are the parameters obtained at the CCSD(T) level of theory by extrapolating to the CBS limit and including CV corrections; CBS_{best} refers to the best-estimated equilibrium structure derived by including fT and fQ corrections.
[b] Minimum structure of the potential energy surface obtained at the CCSD(T)/CBS+CV+HO (up to CCSDTQ(P))+SR+DBOC level. Readers are referred to Ref. 43 for details.
[c] fc-CCSD(T)/cc-pV(Q,5)Z structure including CV correction (computed at the MP2/cc-pwCVQZ level).
[d] In parentheses the uncertainty as derived from the fit or as reported in the article.

following gradient:

$$\frac{dE_{CBS+CV}}{dx} = \frac{dE^{\infty}(HF-SCF)}{dx} + \frac{dE^{\infty}(CCSD(T))}{dx} + \frac{d\Delta E(CV)}{dx} \quad (1)$$

where the first two terms account for the extrapolation to the complete basis set (CBS) limit which is performed separately for HF-SCF and CCSD(T) correlation energies. The extrapolation scheme of Feller [73] and the n^{-3} expression [74] were used for the HF-SCF and CCSD(T) parts, respectively. Since the extrapolation to the CBS limit is carried out within the frozen-core (fc) approximation, the contribution due to CV correlation energy needs to be incorporated. This was estimated by taking the difference between all-electron (ae) and frozen-core (fc) CCSD(T) calculations in the same basis set. The correction terms due to the inclusion of full treatment of triple and quadruple excitations, thereby exploiting the CCSDT [75,76] and CCSDTQ [77–79] methods, were computed using the MRCC software package [80,81] and in conjunction with the cc-pVTZ (for the fT correction, as CCSDT-CCSD(T) difference) and cc-pVDZ (for the fQ correction, as CCSDTQ-CCSDT difference) basis sets, within the fc approximation. Their incorporation into the CBS+CV results leads to the best-estimated equilibrium geometry CBS+CV+fT+fQ, which is hereafter denoted as CBS_{best}.

The harmonic frequencies were computed with the fc-CCSD(T) method combined with the cc-pV5Z basis set for the H and C atoms, and the aug-cc-pV(5+*d*)Z for Cl, hereafter shortly labeled as V5Z-aV(5+*d*)Z, and exploiting the CFOUR implementation of analytic second derivatives [82]. Nuclear quadrupole coupling constants were obtained at the ae-CCSD(T)/cc-pwCV5Z level of theory and were augmented by vibrational corrections at the fc-MP2/aug-cc-pVTZ level of theory computed using the Gaussian 16 suite of programs [83]. Cubic and semi-diagonal quartic force constants were computed at the fc-CCSD(T) level of theory in conjunction with the cc-pVQZ basis set for the H and C atoms, and the cc-pV(*Q*+*d*)Z for Cl; this basis set is hereafter shortly labeled as VQZ-V(*Q*+*d*)Z. These computations were employed in a VPT2 treatment (VPT2 standing for vibrational perturbation theory to second order) to derive the vibrational corrections to the equilibrium rotational constants and to incorporate anharmonicity to the harmonic force field. Concerning the latter point, we employed a hybrid force field approach in a normal-coordinate representation (for further details about the methodology followed here see for example Refs [13–17]) within the framework of VPT2; all these calculations were performed by using an appropriate suite of programs [84] implementing the formulas given in the literature [85–87].

3. Results and discussion

The molecule of mono-deuterated chloromethane (CH_2DCl, symmetry point group C_s) is a nearly-prolate asymmetric-top rotor ($\kappa = -0.99$). The *a*- and *b*- principal axes of inertia define the symmetry plane, being the *c*-axis perpendicular to it. Its nine vibrational normal modes, in terms of their symmetry species, can be grouped as $6A' \oplus 3A''$; the six *A'* vibrations (ν_1 – ν_6) will produce *a*-/*b*-hybrid absorptions, while those having *A''* symmetry (ν_7 – ν_9) will yield *c*-type bands.

3.1. Ab initio equilibrium structure data, rotational analysis, semi-experimental equilibrium geometry, and ro-vibrational parameters

The equilibrium structure of CH_3Cl has been the object of many theoretical investigations (see for example Refs. [42,88] and references therein). The comparison between our CBS_{best} computed values and the most recent ones available in the literature is reported in Table 1. Looking at the data obtained in the present work we note that, moving from CBS+CV to CBS_{best}, the inclusion of the fT and fQ corrections leads to a very small change of the C–Cl bond length (becoming longer by about 0.9 mÅ), while both the C–H bond and the $\beta_{(HCCl)}$ angle remain nearly unchanged. Owens et al. [42] recently reported equilibrium structural parameters of CH_3Cl, obtained from a potential energy surface computed by explicitly correlated coupled cluster calculations with extrapolation to the CBS limit and taking also into account the contributions due to the CV correlation, higher-order (HO) electron correlation terms (up to the contributions due to the perturbative pentuples), the diagonal Born-Oppenheimer corrections (DBOC) and scalar relativistic (SR) effects. The comparison between the equilibrium geometry obtained in Ref. [42] and our CBS_{best} values reveals an excellent agreement, even if the latter are derived without the inclusion of DBOC and SR effects and accounting for HO electron correlation terms up to the fQ corrections, thus pointing out that in our determination all the relevant contributions have been incorporated. For the sake of completeness, we note that at the CBS_{best} level the HCH angle is 110.53°, a value very similar to that reported in Ref. 43 (110.54°). Despite the lower level of theory employed, the values reported in Ref. [88] are very similar to our results, the difference being not greater than 0.5 mÅ for the bond lengths, and about 0.06° for the bond angle. Discrepancies so small are very likely to be ascribed to a compensation of errors: the CV term evaluated at the MP2 level is probably overestimated and thus recovering the missing extrapolation to the CBS limit.

Given the excellent agreement between the CBS_{best} equilibrium parameters obtained in the present work and those reported by Owens et al. [42], we decided to use the former to compute the equilibrium rotational constants for the different isotopologues of CH_2DCl investigated in this work, namely $CH_2D^{35}Cl$, $CH_2D^{37}Cl$, $^{13}CH_2D^{35}Cl$ and $^{13}CH_2D^{37}Cl$; the corresponding data are listed in Table 2. Then, incorporation of the vibrational corrections (as explained in the Computational section) led to the prediction of the ground state rotational constants. These data, together with the

Table 2
Equilibrium rotational constants of different isotopologues of CH_2DCl[a].

	$^{12}CH_2D^{35}Cl$	$^{12}CH_2D^{37}Cl$	$^{13}CH_2D^{35}Cl$	$^{13}CH_2D^{37}Cl$
A_e	121,262.76	121,261.07	121,116.83	121,115.13
B_e	12,574.18	12,371.00	12,152.89	11,947.92
C_e	12,277.13	12,083.35	11,873.79	11,678.04

[a] Values (in MHz) derived from the CBS_{best} geometry reported in Table 1.

computed quartic centrifugal distortion constants derived from the harmonic force at the fc-CCSD(T)/V5Z-AV(5+*d*)Z level of theory, were employed to predict the rotational spectra of $^{13}CH_2D^{35}Cl$ and $^{13}CH_2D^{37}Cl$, previously unknown. Our predictions were then used to search for the most intense a-type R branch transitions in the 250–290 GHz frequency interval and to guide the assignment with great confidence. In fact, thanks to the high accuracy of our theoretical estimates, all the experimental transitions were found less than 10 MHz apart from the predicted position. The measurements include the $J = 11 \leftarrow 10$ and $J = 12 \leftarrow 11$ transitions for both isotopologues and probed energy levels with K_a values up to 9 for $^{13}CH_2D^{35}Cl$ and up to 11 for $^{13}CH_2D^{37}Cl$. The spectral resolution was high enough to observe the chlorine hyperfine structure resolved in most cases. Moreover, we extended the measurements of the rotational spectra of $CH_2D^{35}Cl$ and $CH_2D^{37}Cl$ at higher frequencies by recording and analyzing several transitions in the 360–400 GHz and 480–500 GHz ranges, with the aim of improving and expanding the centrifugal analysis of these two species. In this case, the highest values of the J and K_a quantum number observed are 41 and 19, respectively. The spectroscopic constants, determined from fitting the new and previous measurements by means of the SPFIT subprogram of the CALPGM suite [89], are reported in Table 3. The list of all the observed transitions for the isotopologues investigated in the present work is deposited as supplementary material.

The data listed in Table 3 show an overall excellent agreement between the experimental and the computed values of the rotational constants. The largest deviations are observed for the *A* rotational constants (around 0.04%) while both *B* and *C* predictions are nearly coincident with their experimental counterparts (the deviations being well within 0.5 MHz). The mean absolute percentage errors (MAEs) are not greater than 0.02% for all the different isotopologues investigated. Moving to the quartic centrifugal distortion terms, we observe that for both $CH_2D^{35}Cl$ and $CH_2D^{37}Cl$, all predicted values are in very good agreement with their experimental counterparts, the maximum absolute error being smaller than 5% (MAE less than 3%); a good agreement is also found for the sextic centrifugal distortion constants, as expected from previous benchmark studies [90,91].

We determined a complete semi-experimental equilibrium structure for chloromethane by combining our rotational data with the ones already available in the literature. A total of 28 experimental ground-state rotational constants of different isotopologues have been collected and corrected for the vibrational corrections computed in this work to obtain a set of semi-experimental equilibrium rotational constants. In detail, the experimental rotational constants were taken from both infrared and microwave studies of 12 isotopologues, namely those investigated in the present work ($CH_2D^{35}Cl$, $CH_2D^{37}Cl$, $^{13}CH_2D^{35}Cl$ and $^{13}CH_2D^{37}Cl$) together with $CH_3{}^{35}Cl$ [44], $CH_3{}^{37}Cl$ [44], $^{13}CH_3{}^{35}Cl$ [92], $^{13}CH_3{}^{37}Cl$ [93], $CHD_2{}^{35}Cl$ (our unpublished measurements combined with Ref. [94]), $CHD_2{}^{37}Cl$ (our unpublished measurements combined with Ref. 95), $CD_3{}^{35}Cl$ [95] and $CD_3{}^{37}Cl$ [95]. The structural parameters of chloromethane, namely the H–C-Cl angle and the C–H and C–Cl bond lengths, have been fitted against the 28 moments of inertia associated to our dataset in a least squares procedure. All these parameters, listed in Table 1, have been determined with an excel-

Table 3
Spectroscopic parameters (MHz) of CH_2DCl in the ground vibrational state[a].

	$^{12}CH_2D^{35}Cl$		$^{12}CH_2D^{37}Cl$		$^{13}CH_2D^{35}Cl$		$^{13}CH_2D^{37}Cl$	
Parameter	Exp.	Theor.	Exp.	Theor.	Exp.	Theor.	Exp.	Theor.
A_0	119,836.7427(79)	119,884.39	119,834.908(14)	119,882.65	119,708.2(88)	119,753.06	119,704.7(84)	119,751.24
B_0	12,479.34794(15)	12,479.34	12,278.11097(25)	12,278.07	12,063.111(10)	12,063.22	11,860.0644(16)	11,860.16
C_0	12,177.17255(17)	12,177.40	11,985.46516(21)	11,985.66	11,779.104(10)	11,779.45	11,585.4223(16)	11,585.73
Δ_J	0.01503346(27)	0.0147809	0.01458214(30)	0.014337	0.0141767(67)	0.013944	0.0137366(49)	0.013507
Δ_{JK}	0.1565248(11)	0.155519	0.1520171(18)	0.151057	0.1506042(58)	0.149730	0.1461012(29)	0.145279
Δ_K	1.64989(35)	1.589940	1.6549(12)	1.594520	1.594210 [b]	1.594210	1.598769 [b]	1.598769
δ_J x 10^{-3}	0.366505(58)	0.352462	0.349990(88)	0.336595	0.337(19)	0.320854	0.305771 [b]	0.305771
δ_K	0.024314(77)	0.023144	0.02346(13)	0.022485	0.021744 [b]	0.021744	0.021096 [b]	0.021096
Φ_J x 10^{-9}	−4.530 [b]	−4.530	−4.270 [b]	−4.270	−4.462 [b]	−4.462	−4.239 [b]	−4.239
Φ_{JK} x 10^{-6}	0.3141(39)	0.314	0.3031(38)	0.299	0.286 [b]	0.286	0.269 [b]	0.269
Φ_{KJ} x 10^{-6}	3.7046(80)	3.570	3.5431(73)	3.440	3.61 [b]	3.61	3.455 [b]	3.455
Φ_K x 10^{-3}	0.0767 [b]	0.0767	0.0766 [b]	0.0766	0.0766 [b]	0.0766	0.0763 [b]	0.0763
ϕ_J x 10^{-9}	0.3180 [b]	0.3180	0.305 [b]	0.305	0.271 [b]	0.271	0.256 [b]	0.256
ϕ_{JK} x 10^{-6}	0.0125 [b]	0.0125	0.0118 [b]	0.0118	0.00908 [b]	0.00908	0.00824 [b]	0.00824
ϕ_K x 10^{-3}	0.0109 [b]	0.0109	0.0107 [b]	0.0107	0.0100 [b]	0.0100	0.00980 [b]	0.00980
χ_{aa}(Cl)	−74.488(14)	−72.06	−58.708(18)	−56.92	−74.59(14)	−72.08	−58.850(81)	−56.81
χ_{bb}(Cl)	37.126(29)	35.92	29.295(27)	28.37	35.94 [b]	35.94	28.33 [b]	28.33

[a] Numbers in parentheses are one standard deviation and apply to the last significant digits.
[b] Fixed to the theoretical value.

Table 4
Computed rotational constants (cm^{-1}) for the first vibrational excited states of different isotopologues of CH_2DCl.

Vibrational state	Rotational constant	$^{12}CH_2D^{35}Cl$		$^{12}CH_2D^{37}Cl$		$^{13}CH_2D^{35}Cl$	$^{13}CH_2D^{37}Cl$
		Theor. [a]	Exp. [b]	Theor. [a]	Exp. [b]	Theor. [a]	Theor. [a]
$\nu_1 = 1$	*A*	3.9703785	–	3.9703225	–	3.96682308	3.96676654
	B	0.4162402	–	0.4095322	–	0.40239706	0.39562805
	C	0.4063568	–	0.3999604	–	0.39309895	0.38663593
$\nu_2 = 1$	*A*	3.9649338	–	3.9648713	–	3.96115879	3.96109579
	B	0.4161570	–	0.4094475	–	0.40231823	0.39554788
	C	0.4058141	–	0.3994306	–	0.39259976	0.38614919
$\nu_3 = 1$	*A*	4.0013297	3.9977994 [c]	4.0012834	–	3.99585712	3.99580985
	B	0.4165952	0.4166366 [c]	0.4098669	–	0.40266469	0.39587715
	C	0.4082836	0.4083607 [c]	0.4018182	–	0.39483141	0.38830235
$\nu_4 = 1$	*A*	4.0100635	4.014906 [d]	4.0100050	–	4.00542213	4.00536428
	B	0.4157590	0.41595714 [d]	0.4090460	–	0.40188771	0.39511487
	C	0.4031652	0.40301241 [d]	0.3968496	–	0.39006791	0.38368443
$\nu_5 = 1$	*A*	4.0033186	4.0006281 [c]	4.0035979	4.0008953 [e]	3.99968356	3.99988847
	B	0.4144954	0.41450372 [c]	0.4078483	0.40785304 [e]	0.40081793	0.39409722
	C	0.4043328	0.40452555 [c]	0.3979930	0.39817122 [e]	0.39123215	0.38481731
$\nu_6 = 1$	*A*	3.9959530	3.9938571 [c]	3.9957289	3.9937307 [e]	3.99056434	3.99041208
	B	0.4134214	0.41328964 [c]	0.4067546	0.40663171 [e]	0.39954179	0.39282663
	C	0.4034752	0.40316713 [c]	0.3971254	0.39683473 [e]	0.39021922	0.38381173
$\nu_7 = 1$	*A*	3.9804190	–	3.9803623	–	3.97601267	3.97595538
	B	0.4164889	–	0.4097754	–	0.40263238	0.39585812
	C	0.4063637	–	0.3999695	–	0.39312093	0.38665969
$\nu_8 = 1$	*A*	3.9465752	3.936636 [d]	3.9464836	–	3.94302599	3.94293326
	B	0.4157450	0.41554850 [d]	0.4090426	–	0.40183789	0.39507611
	C	0.4065508	0.40657266 [d]	0.4001374	–	0.39318640	0.38670854
$\nu_9 = 1$	*A*	4.0252833	4.0233803 [c]	4.0250754	4.0232222 [e]	4.02058055	4.02037306
	B	0.4151617	0.41517453 [c]	0.4084594	0.40847734 [e]	0.40133535	0.39457365
	C	0.4047519	0.40473506 [c]	0.3983869	0.39836778 [e]	0.39157145	0.38513924

[a] Theoretical computed values (in cm^{-1}); see text for details.
[b] Experimental values (in cm^{-1}).
[c] Data taken from Ref. 57.
[d] Data taken from Ref. 58.
[e] Data taken from Ref. 60.

lent accuracy, the uncertainty being below 1×10^{-5} Å for the bond lengths and about 1×10^{-3} degrees for the H–C-Cl angle. Moreover, our semi-experimental equilibrium structure is in remarkably good agreement with our best estimate equilibrium structure, thus definitely confirming the quality of our *ab initio* calculations. Compared to our semi-experimental equilibrium structure, the data obtained by Demaison et al. [96] are characterized by a larger H–C-Cl angle, while the structure reported by Jensen et al. [97], often used as reference, is biased by a value of the C–H length (1.0854 Å) which is too long (by more than 2 mÅ) with respect to our data, thus confirming the observations reported by other authors [42,98].

Concerning the excited vibrational states, in Table 4 we report the computed rotational constants for the single excited vibrational states of all isotopologues, together with the corresponding experimental data (when available). The predicted values listed in this Table take into account the same kinds of Coriolis interactions among fundamentals that were investigated by the previous high-resolution studies [55–57,59]; their comparison with the literature data points out an overall good agreement, the MAE being smaller than 0.1%. Finally, in order to support further ro-vibrational spectroscopic high-resolution works, the absolute values of the Coriolis coupling constants are reported as supplementary materials in Tables S1–S4.

3.2. Vibrational analysis

The hybrid force field approach was used to obtain accurate theoretical predictions taking into account both mechanical and electrical anharmonicity effects; the harmonic frequencies (at the fc-CCSD(T)/V5Z-AV(5+*d*)Z level of theory) employed in the hybrid force fields for the different isotopologues of CH_2DCl are reported in Table 5 with an approximate description of each normal mode. For completeness, Table 6 reports the computed anharmonic data (frequencies and intensities) of the fundamentals for all the isotopologues. From the analysis of the medium-resolution (up to 0.1 cm^{-1}) infrared spectra, the experimental values for all the fundamentals of $CH_2D^{35}Cl$ (and for some of $CH_2D^{37}Cl$) were determined and are listed in Table 7 together with the corresponding computed fundamental frequencies. As it can be seen from the survey spectrum reported in Fig. 1, the 500–5000 cm^{-1} region is characterized by the absorptions due to the fundamentals; only increasing the pressure of the sample the features due to some overtone and two-quanta combination bands became clearly visible. Moving to higher wavenumbers, the survey spectrum in Fig. 2 shows how the spectral region above 5000 cm^{-1} mainly contains combinations and/or overtones involving the ν_1, ν_2 and ν_7 fundamentals. The overall assignment of the vibrational states carried out in the present work is listed in Table 7 together with the corresponding predicted values. Concerning the fundamentals, by using the threshold criteria proposed by Martin et al. [99] two different Fermi resonances (FR) were identified: one FR of type-1 (1–2) involving the ν_1 fundamental (related to the CH_2 symmetric stretching) and $2\nu_3$ (the first overtone of ν_3, related to the CH_2 scissoring mode), while the other is a type-2 (1–11) FR coupling the ν_2 band (due to the C-D stretching) and the $\nu_8+\nu_9$ combination. At higher wavenumbers (above 3000 cm^{-1}), we identified other instances of anharmonic resonances involving combination bands in which one quantum of the CH_2 symmetric stretching ($\nu_1 = 1$) is coupled to two quanta of the CH_2 scissoring ($\nu_3 = 2$),

Table 5
Harmonic vibrational frequencies of different isotopologues of CH_2DCl[a].

Harmonic	Symmetry	Description [b]	$^{12}CH_2D^{35}Cl$	$^{12}CH_2D^{37}Cl$	$^{13}CH_2D^{35}Cl$	$^{13}CH_2D^{37}Cl$
ω_1	A'	CH_2 *sym.* stretch	3118.9	3118.9	3112.5	3112.5
ω_2	A'	C-D stretch	2306.2	2306.2	2294.1	2294.1
ω_3	A'	CH_2 scissoring	1474.1	1474.1	1470.9	1470.9
ω_4	A'	CH_2 wag	1296.9	1296.8	1290.3	1290.2
ω_5	A'	C-D i.p. bend	840.8	839.9	832.2	831.4
ω_6	A'	C–Cl stretch	727.9	722.1	714.0	708.0
ω_7	A"	CH_2 *asym.* stretch	3183.8	3183.8	3171.6	3171.6
ω_8	A"	C-D/CH_2 o.o.p. bend	1299.1	1299.0	1297.4	1297.4
ω_9	A"	C-D/CH_2 o.o.p. bend	1003.8	1003.5	996.2	995.8

[a] Harmonic frequencies in cm^{-1}; values obtained at the fc–CCSD(T)/V5Z-aV(5 + *d*)Z level of theory (see text).
[b] Sym. and *asym.* stand for symmetric and asymmetric, respectively; i.p. and o.o.p. stand for in plane and out of plane, respectively.

Table 6
Computed anharmonic data (wavenumbers and intensities) of the fundamentals of different isotopologues of CH_2DCl.

Mode	$^{12}CH_2D^{35}Cl$		$^{12}CH_2D^{37}Cl$		$^{13}CH_2D^{35}Cl$		$^{13}CH_2D^{37}Cl$	
	Wvn [a]	I [b]	Wvn [a]	I [b]	Wvn [a]	I [b]	Wvn [a]	I [b]
ν_1	2992.6	15.37	2992.4	14.85	2986.2	15.69	2986.2	15.69
ν_2	2221.0	5.92	2220.8	5.47	2210.6	5.92	2210.5	5.89
ν_3	1435.4	4.12	1434.8	6.68	1431.3	6.57	1431.1	6.61
ν_4	1269.3	9.21	1269.2	9.71	1263.3	8.45	1263.1	8.50
ν_5	826.7	6.26	825.9	6.39	818.6	4.87	817.9	4.67
ν_6	714.0	18.52	708.3	18.05	700.3	19.05	694.4	18.84
ν_7	3032.4	4.94	3032.4	3.60	3021.7	4.87	3021.7	4.87
ν_8	1267.3	1.99	1267.2	2.00	1265.9	1.97	1265.8	1.97
ν_9	986.6	2.17	986.3	2.45	979.2	2.31	978.8	2.32

[a] Wavenumbers in cm^{-1}.
[b] Intensities in km mol^{-1}.

Table 7
Assigned vibrational states of CH_2DCl: comparison between experimental and theoretical wavenumbers (cm^{-1}).

Mode	Experimental [a]	Theoretical [b]	Mode	Experimental [a]	Theoretical [b]
ν_6	714.1(1)/708.4(1) [c]	714.0/708.3 [c]	$\nu_2+\nu_4$	3493.5(3)	3495.7
ν_5	827.0(1)/826.3(1) [c]	826.7/825.9 [c]	$2\nu_3+\nu_9$	3816(1)	3820.8
ν_9	986.7(1)/986.3(1) [c]	986.6/986.3 [c]	$\nu_1+\nu_9$	3969.33(4) [d]	3971.1
ν_8	1267.7(1)	1267.3	$\nu_7+\nu_9$	4014.67(6) [d]	4012.7
ν_4	1268.3(1)	1269.3	$2\nu_3+\nu_8$	4115(1)	4112.8
$2\nu_6$	1421.0(1)	1419.4	$\nu_1+\nu_8$	4244.51(4) [d]	4249.5
ν_3	1433.8(1)	1434.1	$\nu_3+\nu_7$	4438.77(3) [d]	4443.9
$2\nu_9$	1971.0(1)	1970.2	$\nu_7+2\nu_9$	4990.9(3)	4989.9
$\nu_4+\nu_6$	1979.7(3)	1979.2	$\nu_1+\nu_2$	5205.0(3)	5201.8
$\nu_4+\nu_5$	2091.2(3)	2090.3	$\nu_2+\nu_7$	5264.0(3)	5261.9
ν_2	2224.34(7) [d]	2221.0	$\nu_1+\nu_7$	5910.79(2) [d]	5921.5
$\nu_8+\nu_9$	2258.3(3)	2259.6	$2\nu_7$	6040.39(3) [d]	6031.6
$\nu_3+\nu_9$	2412.235(8) [d]	2411.6	$\nu_1+\nu_5+\nu_7$	6718.8(5)	6712.8
$2\nu_8$	2534.3(3)	2535.3	$\nu_1+\nu_7+\nu_9$	6878.9(5)	6861.4
$\nu_3+\nu_8$	2699.74(3) [d]	2700.3	$\nu_1+\nu_7+\nu_8$	7139(1)	7131.6
$\nu_3+\nu_4$	2700.95(5) [d]	2702.5	$2\nu_1+2\nu_6$	7310(1)	7320.8
$2\nu_3$	2846.3(3)	2849.0	$2\nu_7+2\nu_6$	7438(1)	7428.9
$\nu_3 + 2\nu_6$	2857.74(2) [d]	2850.3	$\nu_1+2\nu_7$	8643.35(8) [d]	8632.0
ν_1	2990.282(7) [d]	2992.3	$3\nu_7$	8896.68(6) [d]	8896.7
ν_7	3035.53(2) [d]	3032.4			

[a] Numbers in parentheses are one standard deviation and apply to the last significant digits.
[b] Theoretical values obtained by hybrid force field computations (see text).
[c] $^{35/37}Cl$ isotopologues splitting.
[d] Derived from the analysis of the partially resolved rotational structure (see text).

thus showing an interaction pattern among polyads analogous to what was observed for other halomethanes (see for example Refs. [100–102], and references therein). For example, a binary combination having one quantum of excitation in the ν_1 vibrational state (as $\nu_1+\nu_8$) interacts with a three quanta combination band having two quanta of excitation for the ν_3 state (as $2\nu_3+\nu_8$). Finally, around 6000 cm^{-1} we identified the $2\nu_3+\nu_1$/ $2\nu_1$/ $2\nu_7$ interacting polyad, involving also a 2–2 Darling-Dennison (DD) resonance [103,104] between the $2\nu_1$ and $2\nu_7$ bands. All these anharmonic couplings were treated following the procedure described in Ref. 14 and references therein.

3.2.1. The 500–1500 cm^{-1} spectral region

The spectral region below 1000 cm^{-1} is characterized by the absorptions due to ν_6, ν_5 and ν_9. All these three bands show the $^{35/37}Cl$ isotopologue splitting features, more discernible in the case of the lowest fundamental ν_6 (centered at 714.1/708.4 cm^{-1}). Regarding their intensities, ν_5 (centered at 827.0/826.3 cm^{-1}) and ν_9 (centered at 986.7/986.3 cm^{-1}) appear weaker than ν_6, in line with the corresponding predicted values listed in Table 6. For these three bands, Table 7 points out an excellent agreement between the experimental and computed data, with deviations not greater than 0.4 cm^{-1}. Above 1000 cm^{-1}, the stronger features correspond

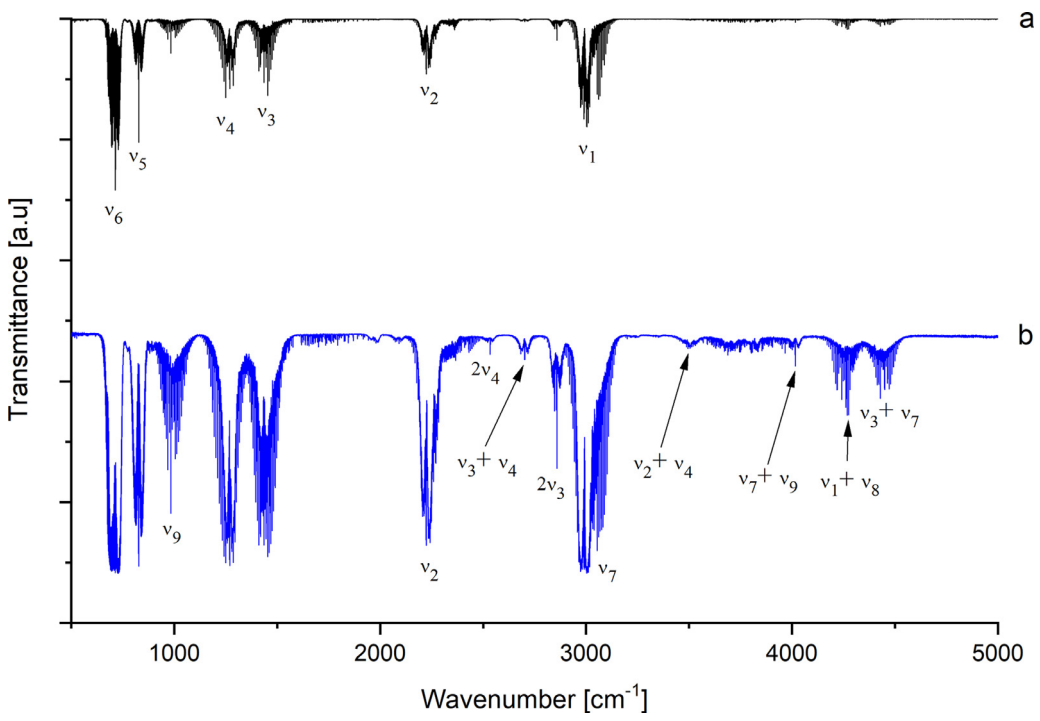

Fig. 1. Gas-phase survey spectra of CH_2DCl in the spectral region 500–5000 cm^{-1}. (a) Resolution = 0.2 cm^{-1}, room temperature, optical path length = 6 m, P = 1.7 kPa; (b) resolution = 0.5 cm^{-1}, room temperature, optical path length = 0.16 m, P = 12.5 kPa. Both traces were vertically shifted for clarity. Only some relevant absorptions are labeled.

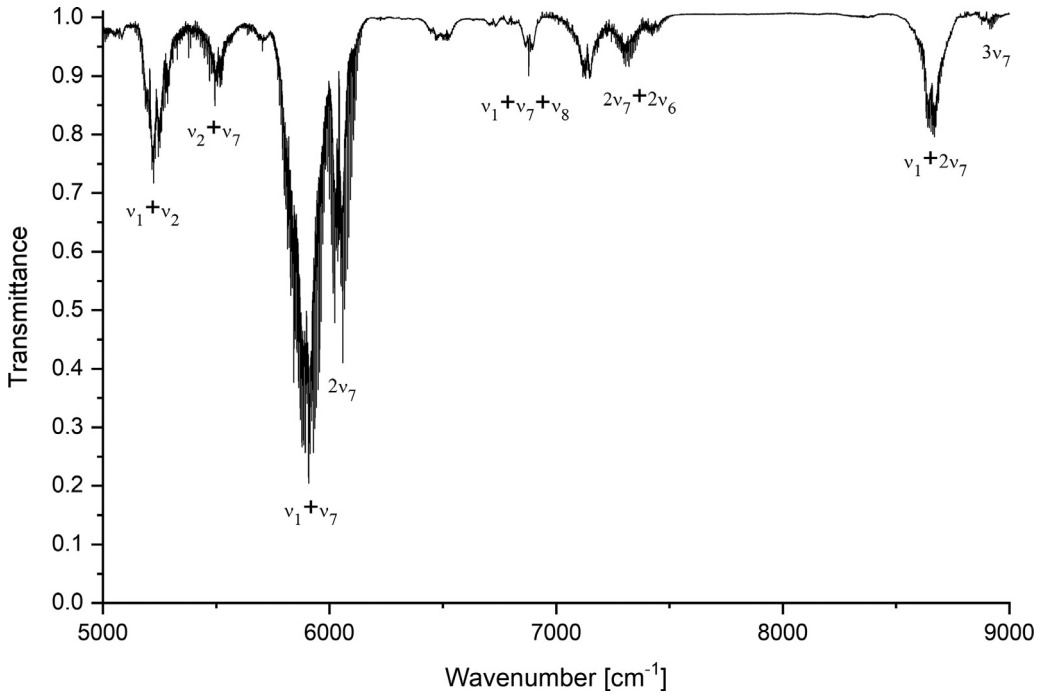

Fig. 2. Gas-phase survey spectrum of CH_2DCl in the spectral region 5000–9000 cm^{-1}. Resolution = 0.5 cm^{-1}, room temperature, optical path length = 37.5 m, P = 2.1 kPa. Only some relevant absorptions are labeled.

to ν_4 (1268.3 cm^{-1}) and ν_3 (1433.8 cm^{-1}), with computed intensities of about 4 and 9 km mol^{-1}, respectively, while the ν_8 fundamental (at 1267.1 cm^{-1}) is weaker (with a predicted intensity of about 2 km mol^{-1}, see Table 6). Besides these strong features, we assigned the first overtone of ν_6 at 1421.0 cm^{-1}. It is worthwhile to note that also for these bands the predicted data show a remarkable agreement with the experimental values, the maximum deviation being smaller than 2 cm^{-1}. Considering all the signals falling in this spectral region, the overall MAE is only 0.7 cm^{-1}.

3.2.2. The 1500–3200 cm^{-1} spectral region

In the 1500–3200 cm^{-1} range, the dominant features are the ν_2 and ν_1 bands. By increasing the sample pressure, many absorptions due to the ν_7 fundamental, to two- and three-quanta combination

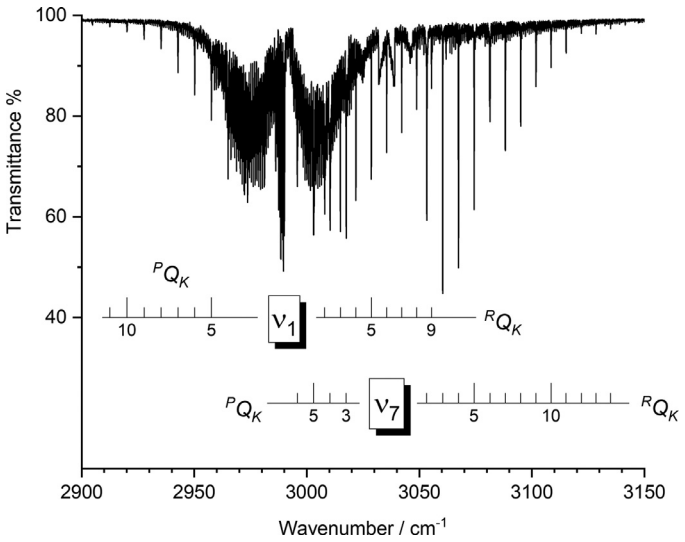

Fig. 3. Gas-phase spectrum of CH_2DCl in the spectral region 2900–3250 cm^{-1}. Resolution = 0.1 cm^{-1}, room temperature, optical path length = 0.16 m, P = 1.3 kPa. The assignments of $^{P,R}Q_K$ clusters of both ν_1 and ν_7 fundamentals are reported.

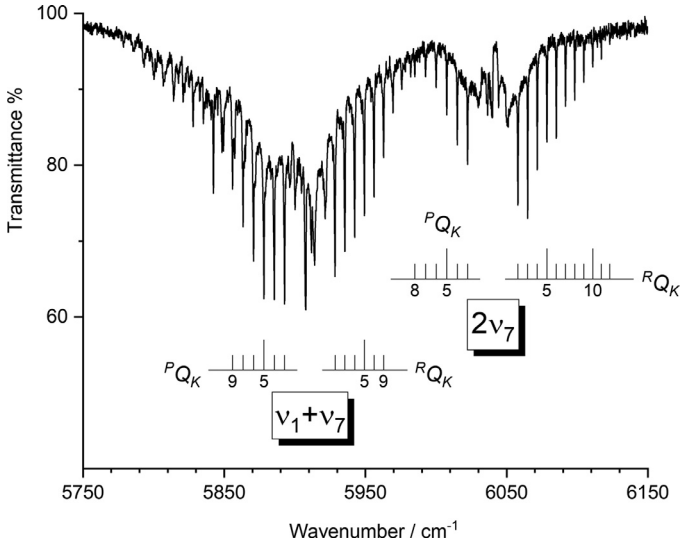

Fig. 4. Gas-phase spectrum of CH_2DCl in the spectral region 5750–6150 cm^{-1}. Resolution = 0.2 cm^{-1}, room temperature, optical path length = 0.16 m, P = 58.5 kPa. The assignments of $^{P,R}Q_K$ clusters of $\nu_1+\nu_7$ and $2\nu_7$ bands are shown.

bands and to the overtones of ν_8 and ν_3 become discernible. It is worthwhile to note that many bands show a partially resolved rotational structure when analyzed at the highest resolutions employed in the present work (0.1 and 0.2 cm^{-1}); an example is reported in Fig. 3, where the $^{P,R}Q_K$ clusters belonging to the ν_1 and ν_7 fundamentals are labeled. The rotational features of *b*- and *c*-type bands were analyzed by a least-square fit and employing the following equation:

$$\nu^{P,R} = \nu_0 + \left(A' - \bar{B}'\right) \mp 2\left(A' - \bar{B}'\right)K + \left[\left(A' - \bar{B}'\right) - \left(A' - \bar{B}'\right)\right]K^2 \pm 4D'_K K^3 \quad (2)$$

with the upper and lower signs referring to the *P*- and *R*-branches, respectively, and $\bar{B} = (B + C)/2$. The data reported in Table 7 point out that the theoretical predictions in this spectral region compare very well with the corresponding experimental data, the overall MAE being about 2 cm^{-1}.

3.2.3. The 3200–5000 cm^{-1} spectral region

The range 3200–5000 cm^{-1} comprises features coming mainly from binary combinations involving the ν_1 and/or ν_7 fundamentals. In this spectral region, many bands show a partially resolved rotational structure, whose clusters were fitted using Eq. (2). We observe that the theoretical predictions are in good agreement with the corresponding experimental data; the maximum deviation is less than 5 cm^{-1}, and the overall MAE is around 3 cm^{-1}. As previously noted, in this spectral region we identified the dyads $2\nu_3+\nu_8/\nu_1+\nu_8$ and $2\nu_3+\nu_9/\nu_1+\nu_9$; after proper treatment of the coupling terms [14], the predicted values for the combination bands involved show deviations of a few wavenumbers with respect to the corresponding experimental data.

3.2.4. The 5000–9000 cm^{-1} spectral region

The last spectral region investigated, 5000–9000 cm^{-1}, is characterized by absorptions mainly due to two- and three-quanta combination bands involving, as in the region discussed previously, ν_1 and/or ν_7 vibrational levels; besides, we identified other signals that were tentatively assigned on the basis of the theoretical predictions. As previously done, the bands showing a partially resolved rotational structure were fitted using Eq. 2; an example is shown in Fig. 4 reporting the absorptions due to $\nu_1+\nu_7$ and $2\nu_7$. The MAE in this range is less than 8 cm^{-1}. We identified three relevant polyads in this spectral region: two centered at about 6000 cm^{-1}, and the last one centered at about 8600 cm^{-1}. The first polyad comprises $2\nu_3+\nu_1/2\nu_1/2\nu_7$. Without any resonances, we predict $2\nu_7$ and $\nu_1+\nu_7$ at 5998 cm^{-1} and 5888 cm^{-1}, respectively, thus being very far from the corresponding experimental values (6040.39 and 5910.79 cm^{-1}, respectively). If we consider only the Darling-Dennison coupling between $2\nu_7$ and $2\nu_1$ (our calculations predict the latter weaker than both $2\nu_7$ and $\nu_1+\nu_7$, and so in the present analysis we considered $2\nu_1$ as "dark state"), the $2\nu_7$ band is shifted up to 6028.2 cm^{-1}, closer to the measured band center. If we assume that $2\nu_3+\nu_1$ is coupled to $2\nu_1$ (that is, in turn, coupled to $2\nu_7$), the treatment of this triad led to a predicted value of 6031.6 cm^{-1} for $2\nu_7$, thus further improving the agreement with the observed value. The other dyad involves $2\nu_3+\nu_7$ and $\nu_1+\nu_7$; without any coupling, as said before our calculations yielded a value of 5888 cm^{-1} for $\nu_1+\nu_7$; assuming a resonance with the $2\nu_3+\nu_7$ dark state, the $\nu_1+\nu_7$ band is shifted up to 5921.5 cm^{-1}, thus leading to a better agreement with the measured band center (5910.79 cm^{-1}).

The last dyad we considered involves $2\nu_7+\nu_1$ (measured band center at 8643.35 cm^{-1}). Without taking into account any resonances our calculations predict this combination at 8734 cm^{-1}, much higher than the measured value, while $3\nu_1$ (too weak to be identified in the spectra) is computed at 8752 cm^{-1}. If we assume an anharmonic resonance between them, the interaction moves $2\nu_7+\nu_1$ down to 8632 cm^{-1}, thus significantly improving the agreement with the experimental data.

Table 7 summarizes all the assignments performed in the present vibrational analysis (together with their estimated uncertainties), and the corresponding predicted values; looking at the overall comparison, the agreement can be considered as very good, with a MAE smaller than 4.0 cm^{-1} for all the assigned absorptions, including also three- quanta combinations and/or overtones, falling in the 600–9000 cm^{-1} spectral range, thus confirming the accuracy of the hybrid force field data here employed.

4. Conclusions

The recent discovery of CH_3Cl in the interstellar medium suggests that also its deuterated species might be present. Here the results of a comprehensive quantum-chemical and experimental investigation focused on the spectroscopic properties of CH_2DCl are presented. Accurate predictions of its equilibrium structure

were obtained by a computational strategy involving calculations at the coupled cluster level of theory, using a complete basis set extrapolation scheme also including the contributions coming from the full treatment of triple and quadruple excitations as well as core-correlation effects. High-level anharmonic data were then used to compute the rotational constants for the ground and vibrational excited states and centrifugal distortion constants for all the four isotopologues investigated.

From the experimental side, we improved the knowledge of the rotational spectrum of CH_2DCl by extending the measurements of $CH_2D^{35}Cl$ and $CH_2D^{37}Cl$ up to 520 GHz as well as by recording the spectra of $^{13}CH_2D^{35}Cl$ and $^{13}CH_2D^{37}Cl$ for the first time. The newly determined set of spectroscopic parameters, namely rotational, centrifugal distortion, and nuclear quadrupole coupling constants, are found in excellent agreement with the corresponding computed values. Finally, by using the ground state constants of 12 isotopologues, we derived a complete and accurate semi-experimental equilibrium structure for chloromethane. Analysing the infrared spectrum at medium resolution, the vibrational features up to 9000 cm^{-1} were identified and assigned, and several polyads involving anharmonic resonances were disentangled. The thorough investigation carried out in this work thus provides accurate spectroscopic data useful for guiding and facilitating the potential detection of the different isotopologues of CH_2DCl by rotational spectroscopy as well as for assisting future high-resolution studies in the infrared region.

Declaration of Competing Interest

The authors declare that they have no known competing financial interests or personal relationships that could have appeared to influence the work reported in this paper.

CRediT authorship contribution statement

Andrea Pietropolli Charmet: Conceptualization, Validation, Formal analysis, Investigation, Data curation, Writing – original draft, Writing – review & editing, Visualization, Supervision, Project administration. **Paolo Stoppa:** Resources, Writing – review & editing. **Alessandra De Lorenzi:** Resources, Writing – review & editing. **Mattia Melosso:** Conceptualization, Validation, Formal analysis, Investigation, Data curation, Writing – original draft, Writing – review & editing, Visualization. **Andrè Achilli:** Formal analysis, Investigation. **Luca Dore:** Resources, Writing – review & editing, Funding acquisition. **Cristina Puzzarini:** Software, Resources, Writing – review & editing, Funding acquisition. **Elisabetta Canè:** Writing – review & editing. **Filippo Tamassia:** Investigation, Validation, Writing – review & editing, Project administration.

Data availability

Data will be made available on request.

Acknowledgments

We gratefully acknowledge the financial support by University Ca' Foscari Venezia (ADiR funds) and by Bologna University (RFO funds). This work has also been supported by MUR (PRIN Grant Number 202082CE3T). The authors also gratefully remember Mr. A. Baldan for the synthesis of the CH2DCl sample. One of the authors (APC) gratefully acknowledges the CINECA (Grants Numbers. HP10CJ2KUM and HP10CUY70O).

Supplementary materials

Supplementary material associated with this article can be found, in the online version, at doi:10.1016/j.jqsrt.2023.108624.

References

[1] Engel A, Rigby M, Burkholder JB, Fernandez RP, Froidevaux L, Hall BD, Hossaini R, Saito T, Vollmer MK, Yao B. Update on ozone-depleting substances (ODS) and other gases of interest to the Montreal protocol. Scientific assessment of ozone depletion: 2018, Geneva, Switzerland: World Meteorological Organization; 2018. ch.1.
[2] David E, Niculescu VC. Volatile organic compounds (VOCs) as environmental pollutants: occurrence and mitigation using nanomaterials. Int J Environ Res Public Health 2021;18:13147. doi:10.3390/ijerph182413147.
[3] Dai C, Zhou Y, Peng H, Huang S, Qin P, Zhang J, Yang Y, Luo L, Zhang X. Current progress in remediation of chlorinated volatile organic compounds: a review. J Ind Eng Chem 2018;62:106–19.
[4] Huang B, Lei C, Wei C, Zeng G. Chlorinated volatile organic compounds (Cl-VOCs) in environment - sources, potential human health impacts, and current remediation technologies. Environ Int 2014;71:118–38.
[5] Lou X, Feng Y, Yang S, Dong Y. Ultra-wide-dynamic-range gas sensing by optical pathlength multiplexed absorption spectroscopy. Photon Res 2021;9:193.
[6] Wang Z, Du Y, Ding Y, Peng Z. A wide-range and calibration-free spectrometer which combines wavelength modulation and direct absorption spectroscopy with cavity ringdown spectroscopy. Sensors 2020;20:585. doi:10.3390/s20030585.
[7] De A, Dutta Banik G, Maity A, Pal M, Pradhan M. Continuous wave external–cavity quantum cascade laser-based high resolution cavity ring-down spectrometer for ultrasensitive trace gas detection. Opt Lett 2016;41:1949–52.
[8] McNaughton D, Robertson EG, Thompson CD, Chimdi T, Bane MK, Appadoo D. Overview of high-resolution infrared measurement and analysis for atmospheric monitoring of halocarbons. Anal Chem 2010;82:7958–64.
[9] Barone V, Alessandrini S, Biczysko M, Cheeseman JR, Clary DC, McCoy AB, et al. Computational molecular spectroscopy. Nat Rev Methods Primers 2021;1:38. doi:10.1038/s43586-021-00034-1.
[10] Barone V, Puzzarini C, Mancini G. Integration of theory, simulation, artificial intelligence and virtual reality: a four-pillar approach for reconciling accuracy and interpretability in computational spectroscopy. Phys Chem Chem Phys 2021;23:17079–96.
[11] Puzzarini C, Bloino J, Tasinato N, Barone V. Accuracy and interpretability: the devil and the holy grail. new routes across old boundaries in computational spectroscopy. Chem Rev 2019;119:8131–91.
[12] Gambi A, Pietropolli Charmet A, Stoppa P, Tasinato N, Ceselin G, Barone V. Molecular synthons for accurate structural determinations: the equilibrium geometry of 1-chloro-1-fluoroethene. Phys Chem Chem Phys 2019;21:3615–25.
[13] Pietropolli Charmet A, Ceselin G, Stoppa P. Tasinato N The spectroscopic characterization of halogenated pollutants through the interplay between theory and experiment: application to R1122. Molecules 2022;27:748. doi:10.3390/molecules27030748.
[14] Pietropolli Charmet A, Stoppa P, Tasinato N, Giorgianni S, Gambi A. Study of the vibrational spectra and absorption cross sections of 1-chloro-1-fluoroethene by a joint experimental and *Ab initio* approach. J Phys Chem A 2016;120:8369–86.
[15] Tasinato N, Pietropolli Charmet A, Stoppa P, Giorgianni S, Gambi A. Quantum–chemical ab initio investigation of the vibrational spectrum of halon 1113 and its anharmonic force field: a joint experimental and computational approach. Chem Phys 2012;397:55–64.
[16] Carnimeo I, Puzzarini C, Tasinato N, Stoppa P, Pietropolli Charmet A, Biczysko M, et al. Anharmonic theoretical simulations of infrared spectra of halogenated organic compounds. J Chem Phys 2013;139:074310. doi:10.1063/1.4817401.
[17] Demaison J, Møllendal H, Perrin A, Orphal J, Kwabia Tchana F, Rudolph HD, Willaert F. Microwave and high resolution infrared spectra of vinyl chloride, ab initio anharmonic force field and equilibrium structure. J Mol Spectrosc 2005;232:174–85.
[18] Park JH, Zander R, Farmer CB, Rinsland CP, Russell JM, Horton RH, Raper OF. Spectroscopic detection of CH_3Cl in the upper troposphere and lower stratosphere. Geophys Res Lett 1986;13:765–8.
[19] Kaley AW, Weigum N, McElcheran C, Taylor JR. Global methyl chloride measurements from the ace-fts instrument. International Symposium on Molecular Spectroscopy Department of Chemistry the Ohio State University; 2009. TI-09.
[20] Brown AT, Volk CM, Schoeberl MR, Boone CD, Bernath PF. Stratospheric lifetimes of CFC-12, CCl_4, CH_4, CH_3Cl and N_2O from measurements made by the atmospheric chemistry experiment-fourier transform spectrometer (ACE-FTS). Atmos Chem Phys 2013;13:6921–50.
[21] Sun J, Xin J, Hu B, Song T, Wang L, Wu F, et al. The spatial-temporal distribution characteristics of atmospheric chloromethane according to data from the CARE-China network. Atm Env 2021;260:118484. doi:10.1016/j.atmosenv.2021.118484.
[22] Umezawa T, Baker AK, Brenninkmeijer CAM, Zahn A, Oram DE, van Velthoven PFJ. Methyl chloride as a tracer of tropical tropospheric air in the lowermost stratosphere inferred from IAGOS-CARIBIC passenger aircraft measurements. J Geophys Res Atmos 2015;120:313–26.
[23] Shechner M, Guenther A, Rhew R, Wishkerman A, Li Q, Blake D, Lerner G, Tas E. Emission of volatile halogenated organic compounds over the various Dead Sea landscapes. Atmos Chem Phys 2019;19:7667–90.
[24] Keppler F, Röhling AN, Jaeger N, Schroll M, Hartmann SC, Greule M. Sources and sinks of chloromethane in a salt marsh ecosystem: constraints from con-

centration and stable isotope measurements of laboratory incubation experiments. Environ Sci Proc Impacts 2020;22:627–41.
[25] Andreae MO, Merlet P. Emission of trace gases and aerosols from biomass burning. Global Biogeochem Cycles 2001;15:955–66.
[26] Li S, Park MK, CO J, Park S. Emission estimates of methyl chloride from industrial sources in China based on high frequency atmospheric observations. J Atmos Chem 2017;74:227–43.
[27] Keppler F, Fischer J, Sattler T, Polag D, Jaeger N, Schöler HF, Greule M. Chloromethane emissions in human breath. Sci Total Environ 2017;605–606:405–10.
[28] Schwieterman EW, Kiang NY, Parenteau MN, Harman CE, DasSarma S, Fisher TM, Arney GN, Hartnett HE, Reinhard CT, Olson SL, Meadows VS, Cockell CS, Walker SI, Grenfell JL, Hegde S, Rugheimer S, Hu R, Lyons TW. Exoplanet biosignatures: a review of remotely detectable signs of life. Astrobiology 2018;18:663–708.
[29] Ben Fathallah O, Manceron L, Dridi N, Rotger M, Aroui H. N_2-, O_2- and Air-broadened half-widths and line shifts of methyl chloride in the 10 μm region. J Quant Spectrosc Radiat Transf 2021;262:107509. doi:10.1016/j.jqsrt.2021.107509.
[30] Dridi N, Manceron L, Ben Fathallah O, Rotger M, Aroui H. O_2- and N_2-broadening parameters in the ν_3 and $2\nu_3$-ν_3 bands of methyl chloride. J Quant Spectrosc Radiat Transf 2020;253:107180. doi:10.1016/j.jqsrt.2020.107180.
[31] Dridi N, Manceron L, Hmida F, Rotger M, Aroui H. Line intensity parameters in the ν_3 and $2\nu_3$-ν_3 bands of methyl chloride in the 13 μm region. J Quant Spectrosc Radiat Transf 2020;251:107306. doi:10.1016/j.jqsrt.2020.107036.
[32] Fathallah O, Manceron L, Dridi N, Rotger M, Aroui H. Line intensities and self-broadening coefficients of methyl chloride in the 10 μm region. J Quant Spectrosc Radiat Transf 2020;242:106777. doi:10.1016/j.jqsrt.2019.106777.
[33] Sylvain L, Lepère M. N_2-collisional broadening coefficients of lines in the ν_2 band of chloromethane from low to room temperature. J Mol Spectrosc 2020;369:111269. doi:10.1016/j.jms.2020.111269.
[34] Dridi N, Maaroufi N, Manceron L, Rotger M, Aroui H. Measurement and modeling of self-broadening coefficients of the ν_3 and $2\nu_3$-ν_3 bands of methyl chloride. J Quant Spectrosc Radiat Transf 2019;235:108–19.
[35] Nikitin AV, Dmitrieva TA, Gordon IE. Improved spectroscopic line list of methyl chloride in the 1900–2600 cm^{-1} spectral region. J Quant Spectrosc Radiat Transf 2016;177:49–58.
[36] Lucchesini A, Gozzini S. Diode laser spectroscopy of methyl chloride overtones at 850–860 nm. J Quant Spectrosc Radiat Transf 2016;168:170–5.
[37] Barbouchi Ramchani A, Jacquemart D, Dhib M, Aroui H. Line positions, intensities and self-broadening coefficients for the ν_5 band of methyl chloride. J Quant Spectrosc Radiat Transf 2013;120:1–15.
[38] Bray C, Perrin A, Jacquemart D, Lacome N. The ν_1, ν_4 and $3\nu_6$ bands of methyl chloride in the 3.4-μm region: line positions and intensities. J Quant Spectrosc Radiat Transf 2011;112:2446–62.
[39] Owens A, Yachmenev A, Thiel W, Fateev A, Tennyson J, Yurchenko SN. EXOMOL line lists – XXIX. The rotation-vibration spectrum of methyl chloride up to 1200 K. MNRAS 2018;479:3002–10.
[40] Owens A, Yurchenko SN, Yachmenev A, Tennyson J, Thiel W. A global ab initio dipole moment surface for methyl chloride. J Quant Spectrosc Radiat Transf 2016;184:100–10.
[41] Wallington TJ, Pasquini Pivesso B, Moura Lira A, Anderson JE, Nielsen CJ, Andersen NH, Hodnebrog Ø. CH_3Cl, CH_2Cl_2, $CHCl_3$, and CCl_4: infrared spectra, radiative efficiencies, and global warming potentials. J Quant Spectrosc Radiat Transf 2016;174:56–64.
[42] Owens A, Yurchenko SN, Yachmenev A, Tennyson J, Thiel W. Accurate ab initio vibrational energies of methyl chloride. J Chem Phys 2015;142:244306. doi:10.1063/1.4922890.
[43] Střítеská LN, Šimečková M, Kania P, Musil P, Kolesniková L, Koubek J, Urban S. Precise ground state molecular parameters of chloromethane. J Mol Struct 2009;919:89–93.
[44] Nikitin A, Champion JP. New ground state constants of $^{12}CH_3{}^{35}Cl$ and $^{12}CH_3{}^{37}Cl$ from global polyad analysis. J Mol Spectrosc 2005;230:168–73.
[45] Neufeld DA, Wolfire MG. The chemistry of interstellar molecules containing the halogen elements. ApJ 2009;706:1594. doi:10.1088/0004-637X/706/2/1594.
[46] Fayolle EC, Öberg KI, Jørgensen JK, Altwegg K, Calcutt H, Müller HSP, Rubin M, van der Wiel MHD, Bjerkeli P, Bourke TL, et al. Protostellar and cometary detections of organohalogens. Nat Astron 2017;1:703–8.
[47] Agbaglo D, Fortenberry RC. Quantum chemical rovibrational characterization of CH_2ClH^+, a low-energy isomer of ionized chloromethane. ACS Earth Space Chem 2019;3:1296–301.
[48] Nguyen QLD, Peters WK, Fortenberry RC. Highly-excited state properties of cumulenone chlorides in the vacuum-ultraviolet. Phys Chem Chem Phys 2020;22:11838–49.
[49] Lin MY, Huang TP, Wu PZ, Chin CH, Wu YJ. Formation of halogen-bearing species. II. irradiation of chloromethane in carbon monoxide ice with VUV light and electrons. ApJ 2020;888:39. doi:10.3847/1538-4357/ab5949.
[50] Coutens A, Vastel C, Caux E, Ceccarelli C, Bottinelli S, Wiesenfeld L. A study of deuterated water in the low-mass protostar IRAS 16293-2422. Astron Astrophys 2012;539:A132. doi:10.1051/0004-6361/201117627.
[51] Melosso M, Bizzocchi L, Sipilä O, Giuliano BM, Dore L, Tamassia F, et al. First detection of NHD and ND_2 in the interstellar medium: amidogen deuteration in IRAS 16293-2422. Astron Astrophys 2020;641:A153. doi:10.1051/0004-6361/202038490.
[52] Bacmann A, Faure A, Hily-Blant P, Kobayashi K, Ozeki H, Yamamoto S, Pagani L, Lique F. Deuterium fractionation of nitrogen hydrides: detections of NHD and ND_2. MNRAS 2020;499:1795–804.
[53] Calcutt H, Jørgensen J, Müller H, Kristensen L, Coutens A, Bourke T, et al. The ALMA-PILS survey: complex nitriles towards IRAS 16293-2422. Astron Astrophys 2018;616:A90. doi:10.1051/0004-6361/201732289.
[54] Wallström SHJ, Muller S, Roueff E, Le Gal R, Black JH, Gérin M. Chlorine-bearing molecules in molecular absorbers at intermediate redshifts. A&A 2019;629:A128. doi:10.1051/0004-6361/201935860.
[55] Baldacci A, Stoppa P, Charmet Pietropolli, Giorgianni S, Nivellini G. High resolution FTIR study of the ν_5 and ν_6 bands of $CH_2D^{35}Cl$: analysis of resonances and determination of ground and upper state constants. Mol Phys 2005;103:2803–11.
[56] Baldacci A, Visinoni R, Giorgianni S, Nivellini G. High-resolution FTIR spectroscopy of $CH_2D^{35}Cl$: rovibrational analysis of the ν_3, ν_9 fundamentals and the $2\nu_6 - \nu_6$, $\nu_5 + \nu_6 - \nu_6$ hot bands. Mol Phys 2008;106:1233–40.
[57] Baldacci A, Visinoni R, Nivellini G. High-resolution FTIR spectroscopy of $CH_2D^{35}Cl$: analysis of the nearly degenerate ν_4 and ν_8 levels. Mol Phys 2010;108:2395–410.
[58] Melosso M, Achilli A, Tamassia F, Canè E, Pietropolli Charmet A, Stoppa P, et al. High-resolution millimeter-wave spectroscopy of CH_2DCl: paving the way for future astronomical observations of chloromethane isotopologues. J Quant Spectrosc Radiat Transf 2020;248:106982. doi:10.1016/j.jqsrt.2020.106982.
[59] Stoppa P, Pietropolli Charmet A, De Lorenzi A, Tamassia F, Melosso M, Canè E, et al. High resolution FTIR study of the ν_5, ν_6, and ν_9 fundamental bands of $CH_2D^{37}Cl$. J Quant Spectrosc Radiat Transf 2021;270:107719. doi:10.1016/j.jqsrt.2021.107719.
[60] Canè E, Villa M, Tarroni R, Tamassia F, Pietropolli Charmet A, Tasinato N, Stoppa P, Giorgianni S. The ro-vibrational analysis of the ν_4 fundamental band of CF_3Br from jet-cooled diode laser and FTIR spectra in the 8.3-μm region. Mol Phys 2014;112:1899–909.
[61] Canè E, Di Lonardo G, Fusina L, Nivellini G, Tamassia F, Villa M. Infrared spectroscopy of $^{15}ND_3$: the ν_2 and ν_4 bending fundamental bands. J Quant Spectrosc Radiat Transf 2013;119:1–11.
[62] Melosso M, Conversazioni B, Esposti CD, Dore L, Canè E, Tamassia F, Bizzocchi L. The pure rotational spectrum of $^{15}ND_2$ observed by millimetre and submillimetre-wave spectroscopy. J Quant Spectrosc Radiat Transf 2019;222:186–9.
[63] Melosso M, Bizzocchi L, Tamassia F, Esposti CD, Canè E, Dore L. The rotational spectrum of ^{15}ND. Isotopic-independent dunham-type analysis of the imidogen radical. Phys Chem Chem Phys 2019;21:3564–73.
[64] Heckert M, Kállay M, Gauss J. Molecular equilibrium geometries based on coupled-cluster calculations including quadruple excitations. Mol Phys 2005;103:2109–15.
[65] Heckert M, Kállay M, Tew DP, Klopper W, Gauss J. Basis-set extrapolation techniques for the accurate calculation of molecular equilibrium geometries using coupled-cluster theory. J Chem Phys 2006;125:044108. doi:10.1063/1.2217732.
[66] Raghavachari K, Trucks GW. A fifth-order perturbation comparison of electron correlation theories. Chem Phys Lett 1989;157:479–83.
[67] Matthews DA, Cheng L, Harding ME, Lipparini F, Stopkowicz S, Jagau T-C, et al. Coupled-cluster techniques for computational chemistry: the CFOUR program package. J Chem Phys 2020;152:214108. doi:10.1063/5.0004837.
[68] Stanton J.F., Gauss J., Harding M.E., Szalay P.G. CFOUR A Quantum Chemical Program Package 2016 With Contributions from Auer AA, Bartlett R.J., Benedikt U., Berger C., Bernholdt D.E., Bomble Y.J., Christiansen O., Engel F., Heckert M., Heun O., Huber C., Jagau T.-C, Jonsson D., Jusélius J., Klein K., Lauderdale W.J., Lipparini F., Matthews D., Metzroth T., Mück L.A., O'Neill D.P., Price D.R., Prochnow E., Puzzarini C., Ruud K., Schiffmann F., Schwalbach W., Stopkowicz S., Tajti A., Vázquez J., Wang F., Watts J.D., and the Integral Packages MOLECULE (Almlöf J, and Taylor P R), PROPS (Taylor P R), ABACUS (Helgaker T, Jensen HJ, Jørgensen P, and Olsen J), and ECP Routines by Mitin AV, and van Wüllen C. For the Current Version see https://cfour.uni-mainz.de/cfour/index.php?n=Main.Bibliography.
[69] Dunning TH Jr.. Gaussian basis sets for use in correlated molecular calculations. I. the atoms boron through neon and hydrogen. J Chem Phys 1989;90:1007–23.
[70] Woon DE, Dunning TH Jr.. Gaussian basis sets for use in correlated molecular calculations. III. the atoms aluminum through argon. J Chem Phys 1993;98:1358–71.
[71] Peterson KA, Dunning TH Jr.. Accurate correlation consistent basis sets for molecular core-valence correlation effects: the second row atoms Al-Ar, and the first row atoms B-Ne revisited. J Chem Phys 2002;117:10548–60.
[72] Woon DE, Dunning TH. Gaussian basis sets for use in correlated molecular calculations. V. core-valence basis sets for boron through neon. J Chem Phys 1995;103:4572–85.
[73] Feller D. The use of systematic sequences of wave functions for estimating the complete basis set, full configuration interaction limit in water. J Chem Phys 1993;98:7059–71.
[74] Helgaker T, Klopper W, Koch H, Noga J. Basis-set convergence of correlated calculations on water. J Chem Phys 1997;106:9369–646.
[75] Noga J, Bartlett RJ. The full CCSDT model for molecular electronic structure. J Chem Phys 1987;86:7041–50.
[76] Scuseria GE, Schaefer HF III.. A new implementation of the full CCSDT model for molecular electronic structure. Chem Phys Letters 1988;152:382–6.

[77] Kucharski SA, Bartlett RJ. Recursive intermediate factorization and complete computational linearization of the coupled-cluster single, double, triple, and quadruple excitation equations. Theor Chim Acta 1991;80:387–405.
[78] Oliphant N, Adamowicz L. Coupled-cluster method truncated at quadruples. J Chem Phys 1991;95:6645–51.
[79] Kucharski SA, Bartlett RJ. The coupled-cluster single, double, triple, and quadruple excitation method. J Chem Phys 1992;97:4282–8.
[80] Kállay M, Nagy PR, Mester D, Rolik Z, Samu G, Csontos J, Csóka J, Szabó PB, Gyevi-Nagy L, Hégely B, Ladjánszki I, Szegedy L, Ladóczki B, Petrov K, Farkas M, Mezei PD, Ganyecz Á. The MRCC program system: accurate quantum chemistry from water to proteins. J Chem Phys 2020;152:074107.
[81] MRCC, a quantum chemical program suite written by Kállay M., Nagy P.R., Mester D., Gyevi-Nagy L., Csóka J., Szabó P.B., Rolik Z., Samu G., Csontos J., Hégely B., Ganyecz Á., Ladjánszki I., Szegedy L., Ladóczki B., Petrov K., Farkas M., Mezei P.D., and Horváth R.A. See https://www.mrcc.hu/index.php/citation.
[82] Gauss J, Stanton JF. Analytic CCSD(T) second derivatives. Chem Phys Lett 1997;276:70–7.
[83] Gaussian 16, Revision C.01, Frisch M.J., Trucks G.W., Schlegel H.B., Scuseria G.E., Robb M.A., Cheeseman J.R., Scalmani G., Barone V., Petersson, G.A., Nakatsuji H., Li X., Caricato M., Marenich A.V., Bloino J., Janesko B.G., Gomperts R., Mennucci B., Hratchian H.P., Ortiz J.V., Izmaylov A.F., Sonnenberg J.L., Williams-Young D., Ding F., Lipparini F., Egidi F., Goings J., Peng B., Petrone A., Henderson T., Ranasinghe D., Zakrzewski V.G., Gao J., Rega N., Zheng G., Liang W., Hada M., Ehara M., Toyota K., Fukuda R., Hasegawa J., Ishida M., Nakajima T., Honda Y., Kitao O., Nakai H., Vreven T., Throssell K., Montgomery J.A. Jr, Peralta J.E., Ogliaro F., Bearpark M.J., Heyd J.J., Brothers E.N., Kudin K.N., Staroverov V.N., Keith T.A., Kobayashi R., Normand J., Raghavachari K., Rendell A.P., Burant J.C., Iyengar S.S., Tomasi J., Cossi M., Millam J.M., Klene M., Adamo C., Cammi R., Ochterski J.W., Martin R.L., Morokuma K., Farkas O., Foresman J.B., Fox D.J. Gaussian, Inc., Wallingford CT, 2016. See https://gaussian.com/gaussian16/.
[84] Pietropolli Charmet A, Cornaton Y. Benchmarking fully analytic DFT force fields for vibrational spectroscopy: a study on halogenated compounds. J Mol Struct 2018;1160:455–62.
[85] Papoušek D, Aliev MR. Molecular vibrational/rotational spectra. Amsterdam, The Netherlands: Elsevier; 1982.
[86] Mills IM, Rao KN, Mathews CW. Vibration-Rotation Structure in Asymmetric- and Symmetric-Top Molecules. In: Molecular spectroscopy: modern research. New York, NY, USA: Academic Press; 1972. p. 115–40. editors.
[87] Aliev MR, Watson JKG, Rao KN. Higher-Order Effects in the Vibration-Rotation Spectra of Semirigid Molecules. In: Molecular spectroscopy: modern research, 3. New York, NY, USA: Academic Press; 1985. p. 2–67. editor.
[88] Demaison J, Margulés L, Boggs JE. The equilibrium C–Cl, C–Br, and C–I bond lengths from Ab initio calculations, microwave and infrared spectroscopies, and empirical correlations. Struct Chem 2003;14:159–74.
[89] Pickett HM. The fitting and prediction of vibration-rotation spectra with spin interactions. J Mol Spectrosc 1991;148:371–7.
[90] Pietropolli Charmet A, Stoppa P, Tasinato N, Giorgianni S. Computing sextic centrifugal distortion constants by DFT: a benchmark analysis on halogenated compounds. J Mol Spectrosc 2017;335:117–25.
[91] Boussessi R, Tasinato N, Pietropolli Charmet A, Stoppa P, Barone V. Sextic centrifugal distortion constants: interplay of density functional and basis set for accurate yet feasible computations. Mol Phys 2020;118:e1734678. doi:10.1080/00268976.2020.1734678.
[92] Constantin FL, Demaison J, Féjard L, Litz M, Bürger H, Pracna P. High-resolution infrared and subterahertz spectroscopy of the $\nu_2 = 1$, $\nu_5 = 1$, and $\nu_3 = 2$ levels of $^{13}CH_3{}^{35}Cl$. J Mol Spectrosc 2007;243:234–44.
[93] Litz M, Bürger H, Féjard L, Costantin FL, Margulès L, Demaison G. Infrared and millimeter-wave studies of $^{13}CH_3Cl$ in the ground, 3^1 and 6^1 states. J Mol Spectrosc 2003;219:238–47.
[94] Mallinson PD. The microwave spectrum of CHD_2Cl. J Mol Spectrosc 1977;68:68–76.
[95] Imachi M, Tanaka T, Hirota E. Microwave spectrum of methyl chloride in the excited vibrational states: coriolis interaction between the ν_2 and ν_5 states. J Mol Spectrosc 1976;63:265–80.
[96] Demaison J, Wlodarczak G, Rudolph HD, Hargittai M, Hargittai I. Advances in molecular structure research, 3. Greenwich: JAI Press; 1997.
[97] Jensen P, Brodersen S, Guelachvili G. Determination of A_0 for $CH_3{}^{35}Cl$ and $CH_3{}^{37}Cl$ from the ν_4 infrared and Raman bands. J Mol Spectrosc 1981;88:378–93.
[98] Demaison J, Wlodarczak G. The equilibrium C-H bond length. Struct Chem 1994;5:57–66.
[99] Martin JML, Lee TJ, Taylor PM, Françojs JP. The anharmonic force field of ethylene, C_2H_4, by means of accurate Ab initio calculations. J Chem Phys 1995;103:2589–602.
[100] Pietropolli Charmet A, Tasinato N, Stoppa P, Giorgianni S, Gambi A. Anharmonic resonances in the CH chromophore overtone spectra of $CHBrF_2$. Mol Phys 2011;109:2163–72.
[101] Horká V, Quack M, Willeke M. Analysis of the CH-chromophore spectra and dynamics in dideutero-methyliodide CHD_2I. Mol Phys 2008;106:1303–16.
[102] Law MM. Joint local- and normal-mode studies of the overtone spectra of the methyl halides: cH_3Cl, CH_3Br, CD_3Br, and CH_3I. J Chem Phys 1999;111:10021–33.
[103] Darling B, Dennison D. The water vapor molecule. Phys Rev 1940;57:128–39.
[104] Rosnik AM, Polik WF. VPT2+K Spectroscopic constants and matrix elements of the transformed vibrational hamiltonian of a polyatomic molecule with resonances using Van Vleck perturbation theory. Mol Phys 2014;112:261–300.